ACS APPLIED MATERIALS & INTERFACES

Research Article

www.acsami.org

Self-Cleaning Membranes from Comb-Shaped Copolymers with Photoresponsive Side Groups

Papatya Kaner,[†] Xiaoran Hu,[‡] Samuel W. Thomas, III,[‡] and Ayse Asatekin*[,†]

[†]Department of Chemical and Biological Engineering, Tufts University, Medford, Massachusetts 02155, United States

[‡]Department of Chemistry, Tufts University, Medford, Massachusetts 02155, United States

Supporting Information

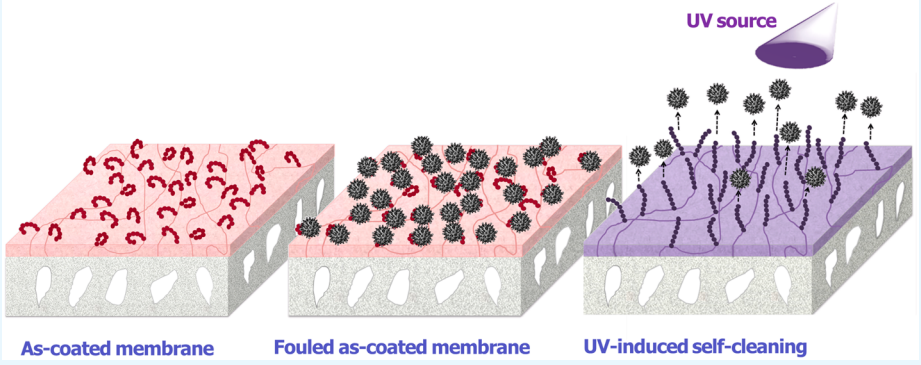

ABSTRACT: In this study, we present a novel self-cleaning, photoresponsive membrane that is capable of removing predeposited foulant layers upon changes in surface morphology in response to UV or visible light irradiation while maintaining stable pore size and water permeance. These membranes were prepared by creating thin film composite (TFC) membranes by coating a porous support membrane with a thin layer of novel comb-shaped graft copolymers at two side-chain lengths featuring polyacrylonitrile (PAN) backbones and photoreactive side chains, synthesized by atom transfer radical polymerization (ATRP). Photoregulated control over membrane properties is attained through a light-induced transition, where the side chains switch between a hydrophobic spiropyran (SP) state and a zwitterionic, hydrophilic merocyanine (MC) state. The light-induced switch between the SP and MC forms changes surface hydrophilicity and causes morphological changes on the membrane surface as evidenced by atomic force microscopy (AFM). Before any phototreatment, the as-coated membrane surface comprises mostly hydrophobic SP groups that allow the adsorption of organic solutes such as proteins the membrane surface, reducing flow rate. Once exposed to UV light, conversion of the SP groups to hydrophilic MC groups leads to the release of adsorbed molecules and the full recovery of the initial water flux. A fouled membrane in the more hydrophilic MC form is also capable of self-cleaning upon conversion to the less hydrophilic SP form by visible light irradiation. The self-cleaning behavior observed for this system, where the surface became less hydrophilic but also experienced a morphological change, demonstrates a novel mechanism that has a mechanical component in addition to the changes in hydrophilicity. It is also the first report, to our knowledge, of self-cleaning performance accompanied by a decrease in hydrophilicity.

KEYWORDS: *self-cleaning, photoresponsive membrane, spiropyran, comb copolymer, fouling resistant, water treatment*

1. INTRODUCTION

Water scarcity affects one in three people globally.[1] Water purification involves the removal of undesired chemicals, biomolecules, ions, salts, minerals, and solid waste from contaminated water. Membrane filtration is an important and promising method for water purification, reclamation, and reuse. Membranes of various pore sizes can be used for a wide range of objectives, from simply removing disease-causing microorganisms[2] to desalination by reverse osmosis.[3−5] Membranes also serve as an efficient, simple, scalable separation method in various industries such as food and beverage, dairy, and bio/pharmaceutical industries.[6−8]

Membrane operations for any application suffer from three major obstacles: low flux, poor selectivity, and fouling. Membranes with high flux (or permeability) are desired because this allows operating at lower pressures or using smaller membrane areas. Membranes also need to have good and stable selectivity, so they can reliably remove undesired components. In either case, higher permeability means better energy efficiency and lower costs. Fouling, simplistically described as the loss of permeability of the membrane due to the adsorption and adhesion of feed components on its surface,[9−11] can lead to very significant losses in productivity,

Received: February 2, 2017
Accepted: March 27, 2017
Published: March 27, 2017

DOI: 10.1021/acsami.7b01585
ACS Appl. Mater. Interfaces 2017, 9, 13619−13631

increasing energy use, cleaning and membrane replacement costs, chemical use, and downtime.[11−13]

One promising approach for modulating membrane performance and protein adsorption involves the use of polymeric materials whose surface chemistry changes from hydrophobic to hydrophilic in response to external stimuli[14] such as temperature,[15,16] pH,[17,18] magnetic[19] or electric fields,[20] ionic strength,[21,22] or light.[23−25] The switch to the hydrophilic state sometimes entails a large degree of swelling that can serve as a mechanical push for the removal of adsorbed proteins and microorganisms. In this vein, controlling the hydrophilic/hydrophobic state of a membrane surface using external stimuli can be employed to design self-cleaning membrane surfaces and decrease membrane fouling.[26−28] Self-cleaning membrane surfaces can be formed by surface coating or grafting nonpolar hydrophobic polymers such as silicone-based[29] and fluorinated[30,31] responsive polymers.

Light has attracted attention as a stimulus of choice for creating responsive surfaces due to its remote but fast effect on material properties. Spiropyran (SP) is a well-known photochromic group that, in response to UV light irradiation, undergoes a photoreversible isomerization from the neutral hydrophobic SP form to a zwitterionic, hydrophilic merocyanine (MC) form. Zwitterions are molecules that comprise an equal number of covalently bound cations and anions, with overall neutral charge. The unique coexistence of opposite charges bridged through organic spacers provides zwitterions extremely high polarity. This feature leads to exceptional antifouling properties for zwitterionic materials; they are highly resistant to the adsorption of proteins and other biomolecules from aqueous solutions.[32−35] Therefore, the zwitterionic MC form of this photochromic functional group is highly hydrophilic and fouling resistant. In addition, the MC form can return to the initial SP state by visible light irradiation. When integrated into membranes, these features of SP enable photoresponsive membranes whose properties such as solvent permeability[36,37] and surface wettability[38,39] can be controlled. However, approaches designed for self-cleaning, where a deposited foulant layer is removed from the membrane surface in response to light irradiation, have not been explored extensively.

A common approach for imparting photoresponsive behavior to membranes involves grafting spiropyran-containing polymers from a pre-existent membrane surface.[36,37,40] Grafting of these photoresponsive chains can be achieved by photoinitiated grafting (UV and non-UV), redox-initiated grafting, plasma-initiated grafting, thermal grafting, and controlled radical grafting methods such as atom transfer radical polymerization (ATRP) and reversible addition−fragmentation chain transfer (RAFT) polymerization.[14,41] However, surface-initiated grafting can potentially alter the chemical structure and morphology of the membrane's selective layer, which may result in undesired changes in permeability, pore size, and selectivity of the underlying membrane. In addition, this method can be expensive, adding a complicated postprocessing step to membrane manufacture. Coating, on the other hand, is an easier process that can conveniently be scaled up to the roll-to-roll manufacturing systems commonly used in membrane systems. To date, photoresponsive membrane coatings have typically focused on controlling membrane selectivity and permeability.[37,42−44]

Most membranes that change their surface energy in response to light simultaneously exhibit a drastic change in pore size and permeability due to the long photoresponsive polymer chains used in their manufacture. Upon UV irradiation, the grafted photoresponsive polymer chains swell into the membrane pores, decreasing effective pore size and flux. Thus, most studies on SP-containing photoresponsive membranes have focused on tuning the permeability and pore size of the membrane and changing surface hydrophilicity. Similarly, light-induced changes in charge and polarity between the SP and MC forms of spiropyrans have enabled their use in developing gated materials that release guest molecules on demand.[45−49] However, in filtration operations where steady performance is needed, this may not be desired. Furthermore, although some studies show that membranes that display the MC form on their surface foul less than the SP form,[40] to our knowledge, self-cleaning membranes that remove a pre-existing foulant layer upon exposure to light and the mechanisms involved in such a process have not yet been reported. Most studies on self-cleaning membranes to date have focused on titanium dioxide (TiO_2), which generates hydroxyl and oxygen radicals that degrade organic materials upon exposure to UV light.[50−52] TiO_2 is also superhydrophilic and can impart better fouling resistance to membranes. These materials are highly effective, but side reactions associated with the generated radicals may also damage the membrane material, limiting the life and stability of these membranes. To our knowledge, the removal of predeposited fouling layers by a photoresponsive polymer has not been studied.

In this paper, we introduce new self-cleaning, photoresponsive membranes that remove foulant layers upon exposure to UV light, exhibit reversible surface chemistry changes, and sustain stable pore size and permeance. These membranes are prepared by coating a commercial membrane with a thin layer of a comb-shaped copolymer with a hydrophobic polyacrylonitrile (PAN) backbone and short photoresponsive spiropyran methacrylate (SPMA) side chains to create thin film composite (TFC) membranes. In this system, the SPMA groups on the membrane surface switch from a hydrophobic state to a hydrophilic/zwitterionic state upon UV exposure. The comb architecture is important, because the mobility of the side chains allows them to expand and push away foulants. Unlike diblock or multiblock architectures, comb-shaped copolymers can create a dense brush of many short polymer chains on a surface by self-assembly,[53−56] which may enhance fouling resistance.[55,56] The free movement of side chains may also enable greater conformational and morphological changes upon light exposure, which can impart a physical/mechanical component to the self-cleaning process. We show that these membranes exhibit complete self-cleaning upon UV irradiation, fully recovering their initial water flux. Furthermore, partial self-cleaning is observed even during the conversion of the MC groups to the more hydrophobic SP groups by visible light exposure, driven by morphological changes on the membrane surface mechanically removing foulant layers. To the best of our knowledge, this is the first study that demonstrates SP-based membranes can remove preformed fouling layers by a simple, nonmechanical intervention of exposure to UV light. It is also the first report, to our knowledge, of self-cleaning performance accompanied by a decrease in hydrophilicity.

2. EXPERIMENTAL SECTION

2.1. Materials. Acrylonitrile (ACN), α-bromoisobutyryl bromide, azobis(isobutyronitrile) (AIBN), 4-methoxyphenol (MEHQ), copper-

DOI: 10.1021/acsami.7b01585
ACS Appl. Mater. Interfaces 2017, 9, 13619−13631

(I) chloride (CuCl), *N*,*N*,*N*′,*N*′,*N*″-pentamethyldiethylenetriamine (PMDETA), bovine serum albumin (BSA, 66.5 kDa), and phosphate-buffered saline (PBS) were purchased from Sigma-Aldrich (St. Louis, MO, USA). Dimethylformamide (DMF), dimethyl sulfoxide (DMSO), methanol (MeOH), acetone, and isopropanol (IPA) were purchased from VWR (West Chester, PA, USA). Deuterated dimethyl sulfoxide (DMSO-d_6) was obtained from Cambridge Isotope Laboratory (Tewksbury, MA, USA). All chemicals and solvents were of reagent grade and used as received, except ACN, which was purified by passage through a basic activated alumina column. 1′-(2-Methacryloyloxyethyl)-3′,3′-dimethyl-6-nitrospiro(2*H*-1-benzopyran-2,2′-indoline) (SPMA) was synthesized following previous papers by first preparing a hydroxyl-functional spyropyran from the commercially available compound 2,3,3-trimethyl-3*H*-indole and then coupling it with methacroyl chloride to prepare the methacrylate.[57] The brominated monomer 2-aminoethyl methacrylate (BBEM) was prepared by the reaction of 2-hydroxyethyl methacrylate with 2-bromoisobutyryl bromide following published methods,[58] and PVDF400R ultrafiltration membranes purchased from Nanostone Inc. (Oceanside, CA, USA) were used as the base membrane for the polymer coatings.

2.2. Synthesis of Comb Copolymer PAN-*g*-SPMA. A comb-shaped copolymer with a polyacrylonitrile (PAN) backbone and side chains made of photoswitchable SPMA repeat units was synthesized following a two-step reaction scheme. The backbone poly(acrylonitrile-*random*-BBEM) (P(ACN-*r*-BBEM)) was synthesized by the free radical copolymerization of ACN and 2-(2-bromoisobutylryloxy)ethyl methacrylate (BBEM) using AIBN as catalyst. BBEM, ACN, and AIBN were dissolved in dimethylformamide (DMF) in a 25 mL three-necked round-bottom flask. The solution was purged with argon for at least 20 min. The reaction was stirred at 80 °C overnight under an argon atmosphere. Then, the reaction mixture was precipitated into methanol, and the resulting precipitate was collected by filtration. The precipitate was dissolved in ∼10 mL of DMF and precipitated again into a 1:1 mixture of acetone and methanol. After filtration, the polymer collected was dried in a vacuum oven for over 2 days. The white solid copolymer obtained was characterized by ^{1}H NMR (500 MHz, DMSO-d_6) δ 4.30−4.50, 3.60−3.25, 2.25−1.45 (all broad signals). The copolymer was prepared at two compositions, with ACN:BBEM ratios of 105:1 and 144:1 by mole. To estimate the molar mass, dynamic light scattering (DLS) measurements were conducted on 1 mg/mL solutions of the copolymers in DMF (Supporting Information, section S1.1).

P(ACN-*r*-BBEM)-*g*-SPMA (PAN-*g*-SPMA) was synthesized via atom transfer radical polymerization (ATRP) using macroinitiator P(ACN-*r*-BBEM) and SPMA. P(ACN-*r*-BBEM), SPMA, and PMDETA were dissolved in DMF to make a 10−20% solution by weight in a 100 mL Schlenk tube. After three freeze−pump−thaw cycles, the solution was frozen with liquid nitrogen, and CuCl was carefully added into the Schlenk tube under argon protection. The tube was vacuumed for another 10 min, after which the reaction was thawed and stirred overnight at 65 °C under argon. The solution was exposed to air for an hour to oxidize the copper salts, which were then removed by passing the solution through an alumina column. The mixture was precipitated in methanol. The solid collected was extracted against copious methanol over 2 days. After filtration, the purple solid collected was dried in a vacuum oven over 2 days. The copolymer composition and side-chain length were determined using ^{1}H NMR (500 MHz, DMSO-d_6) δ 8.30−7.70, 7.30−6.40, 6.20−5.60, 4.60−3.60, 3.25−3.00, 2.30−1.80, 1.30−0.30 (all broad signals). Peak assignments were adopted from the work of Raymo et al.[59] The copolymer was prepared at two side-chain lengths: 12 and 20 SPMA units per initiating Br, as determined by NMR. In the rest of this paper, the synthesized comb copolymers are named SPMA12 and SPMA20. The molar masses of the comb copolymers were estimated using the molar masses of the backbone copolymers obtained from DLS measurements and the side-chain length obtained from ^{1}H NMR (Supporting Information, section S1.2).

2.3. Preparation of Photoresponsive TFC Membranes with Comb Copolymer Selective Layers by Coating. Membranes were prepared by coating a commercial ultrafiltration support membrane with PAN-*g*-SPMA. The copolymer was dissolved in DMSO to make a 12% solution by weight under overnight stirring at room temperature. A thin layer of copolymer solution was then coated onto a commercial ultrafiltration (UF) membrane using a coating rod calibrated for a 6 μm coating thickness (Gardco). A PVDF400R ultrafiltration membrane, purchased from Nanostone Inc. (Oceanside, CA, USA), was used as the base membrane. Following coating, the membrane was immersed into an isopropanol bath for 1 h to precipitate out the copolymer and afterward stored in a water bath. The nonsolvent, isopropanol, was selected due to its low diffusivity with DMSO to prevent the formation of a porous coating.[9] The membrane manufactured using the copolymer SPMA12 is named M-SPMA12, and the membrane manufactured using the copolymer SPMA20 is named M-SPMA20.

2.4. Water Permeability. All filtration experiments were conducted with an Amicon 8010 stirred, dead-end filtration cell (Millipore) with a cell volume of 10 mL and an effective filtration area of 4.1 cm^2, attached to a 3.5 L dispensing vessel. The cell was stirred at 500 rpm using a stir plate, and a pressure of 10 psi (0.07 MPa) was used. A Scout Pro SP401 balance connected to a Dell laptop was used to automatically measure the permeate weight every 30 s using TWedge 2.4 software (TEC-IT, Austria). The permeate flow occurs one droplet at a time; hence, the measured volume at each data point can vary by 1−2 droplets amounting to 0.05−0.1 mL. In water permeability tests, the membrane was first allowed to stabilize by filtering deionized (DI) water at least overnight under 30 psi (0.21 MPa) of pressure. The end of the stabilization period was taken to be the zero time point in the filtration plots. Following stabilization, the water permeability of the membrane was measured. Then, the cell was opened, the membrane swatch was exposed to UV irradiation, and the water permeability was measured again. This procedure was subsequently repeated for the case of visible light exposure. Each membrane was exposed to two successive UV + visible exposure cycles, and the permeability was measured after each exposure. The irradiation time was fixed as 1 h for the M-SPMA12 membrane and 2 h for the M-SPMA20 membrane. For UV irradiation, a UVP compact and hand-held UV lamp equipped with a 254/356 nm split tube was applied using the 254 nm wavelength section. An incandescent light bulb was used for visible light irradiation (450−550 nm). The membrane surface was kept wet during all exposures, and the light source was held 4 cm above the surface.

2.5. Protein Rejection, Fouling, and Self-Cleaning. The rejection, fouling, and self-cleaning properties of the membranes were studied using the dead-end stirred cell filtration systems described above. All filtration runs were conducted at 10 psi (0.07 MPa) after overnight stabilization at 30 psi (0.21 MPa). Model foulant solution comprised 1 g/L BSA (6.5 kDa) in PBS (H 7.4). To determine the pure water permeability, BSA rejection,and fouling resistance, DI water was first filtered for 2 h to determine the initial flux. Then PBS solution was filtered for 2 h. The foulant solution, 1 g/L BSA (6.5 kDa) in PBS, was filtered for 2 h. The filtrate was used to calculate rejection, which is defined as

$$R = \frac{100(C_f - C_p)}{C_f} \quad (1)$$

were R is the protein rejection (%), C_f is the feed concentration (mg/L), and C_p is the permeate concentration (mg/L). Protein concentration in the feed and filtrate was quantified by measuring the UV absorbance at 280 nm utilizing a Thermo Scientific Genesys 10S UV−vis spectrophotometer equipped with a high-intensity xenon lamp and dual-beam optical geometry. Finally, PBS and then DI water were filtered again to compare fluxes before and after fouling. To test the self-cleaning capability upon light exposure, the five-step BSA fouling cycle was succeeded by light exposure on the fouled membrane surface covered with a thin layer of water and then refiltration of DI water to see the consequent water permeability. This complete procedure was conducted four times on each membrane, starting from the as-coated state and, after each fouling cycle, subjecting the surface

DOI: 10.1021/acsami.7b01585
ACS Appl. Mater. Interfaces 2017, 9, 13619−13631

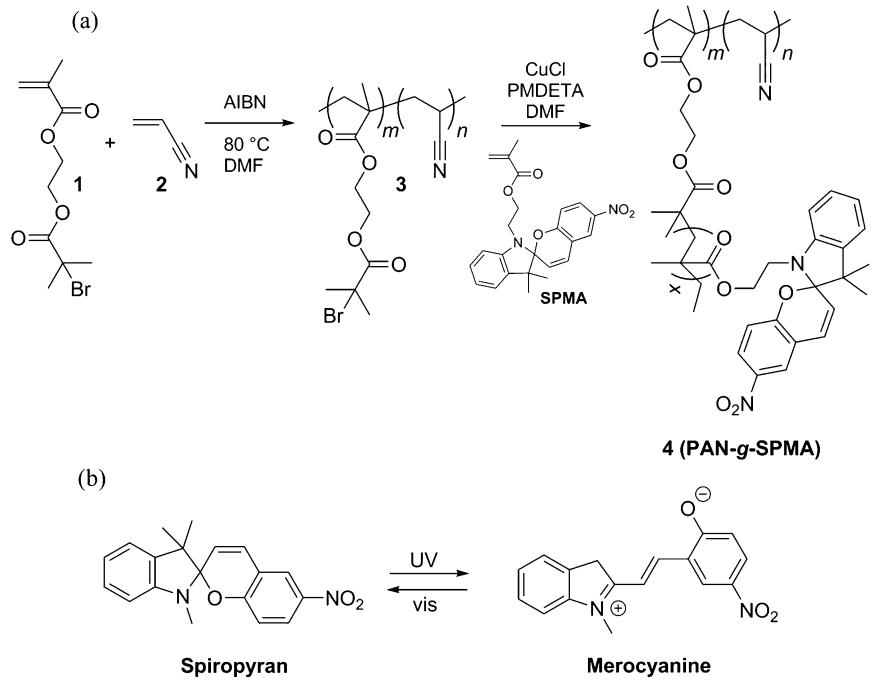

Figure 1. (a) Two-step synthesis scheme for the comb-shaped PAN-*g*-SPMA copolymer and (b) switchable chemistry between the spiropyran and zwitterionic merocyanine.

Table 1. Compositions of the Reaction Mixture and Product Macroinitiator P(ACN-*r*-BBEM)

	reaction mixture composition					copolymer composition
polymer name	BBEM	ACN	AIBN	DMF	yield (%)	ACN:Br mol ratio
105:1 P(ACN-*r*-BBEM)	0.21 g	5.01 g	10.0 mg	20 mL	56	105:1
144:1 P(ACN-*r*-BBEM)	0.11 g	2.68 g	5.0 mg	10 mL	47	144:1

to either UV or visible light treatment on alternate cycles. Light exposure sources and conditions were the same as described previously. As a control experiment, base PVDF400R membrane was also subjected to the five-step BSA fouling cycle followed by UV exposure and then refiltration of DI water to see the consequent water permeability.

2.6. Physical Characterization of Photoresponsive TFC Membranes. Coating layer thickness and surface morphology of the membranes were characterized using a scanning electron microscope (SEM, Phenom G2 Pure Tabletop SEM). Cross sections of the membranes were obtained by first immersing the membrane in liquid nitrogen and then cutting it using a clean razor blade. All samples were sputter-coated with gold–palladium alloy prior to imaging. SEM images of the uncoated PVDF base and the coated membranes were acquired at the same magnification (10,000×).

The switching of the SPMA side chains between SP and MC forms in the copolymer selective layers of the membranes was documented by attenuated total reflection Fourier transform infrared (ATR-FTIR) spectroscopy. The ATR-FTIR spectra were recorded using a Jasco FTIR-6200 spectrometer (Jasco Instruments, Tokyo, Japan), equipped with a deuterated triglycine sulfate detector and a multiple-reflection, horizontal MIRacle ATR accessory. The spectra were analyzed using the instrument's SpectraManager software in absorption mode at 4 cm^{-1} resolution with 256 scans between 2000 and 600 cm^{-1}. Background absorption was subtracted from the sample spectra to establish baseline. The infrared spectra were first collected on the as-coated membranes, followed by measurements on the same membrane upon UV and visible light irradiation in two cycles.

Contact angle (CA) measurements were conducted to follow the changes in surface wettability due to photoinduced conversion between SP and MC units. A Ramé-Hart contact angle instrument (Ramé-Hart Instrument Co.) equipped with a horizontal microscope and camera connected to a video screen was used for the measurements. The membranes were dried for 24 h at room temperature prior to any measurements. The CA was measured first on the as-coated membranes, followed by measurements on the same membrane upon UV and visible light irradiation, respectively. For reference, the CA of the base PVDF400R membrane was also recorded. The volume of each water droplet was 2 μL. The static CA was calculated right after the droplet had been dispensed using the droplet screen image. The dynamic CA was measured as five continuous advancing (θ_A)/receding angles (θ_R) with deionized water. Measurements were repeated using different areas of the membrane; for each result reported, contact angles of at least five water droplets were used.

The surface roughness of the as-coated and UV- and visible light-treated membranes was characterized by AFM (Nanoscope IIIa controller, Bruker). Membrane samples were fixed onto microscopy slides using a double-sided tape. AFM micrographs of 30 × 30 μm^2 surface sections were acquired in tapping mode, and RMS roughness values were obtained directly from scanned images using Gwyddion software. For each RMS roughness result reported, an average value was obtained from at least four 30 × 30 μm^2 surface sections.

3. RESULTS AND DISCUSSION

3.1. Synthesis and Characterization of Copolymers. Figure 1 shows the synthesis scheme for the comb-shaped

DOI: 10.1021/acsami.7b01585
ACS Appl. Mater. Interfaces 2017, 9, 13619–13631

PAN-*g*-SPMA copolymer following a two-step reaction procedure and the switchable chemistry between the spiropyran and zwitterionic merocyanine.

Compound **1**, brominated monomer 2-aminoethyl methacrylate (BBEM), and 1′-(2-methacryloyloxyethyl)-3′,3′-dimethyl-6-nitrospiro(2*H*-1-benzopyran-2,2′-indoline) (SPMA) were synthesized following previous papers.[57,58] P(ACN-*r*-BBEM) (**3**) was synthesized by the free radical copolymerization of the two monomers, brominated BBEM (**1**) and acrylonitrile (ACN) (**2**). Two batches of this copolymer were prepared at different compositions (Table 1). A sample NMR spectrum is shown in Figure 2, with CH protons along the backbone (a) appearing around 3−3.3 ppm, backbone CH_2 protons appearing around 1.9−2.3 ppm, and the CH_2 protons in BBEM (b) appearing around 4.3−4.5 ppm.

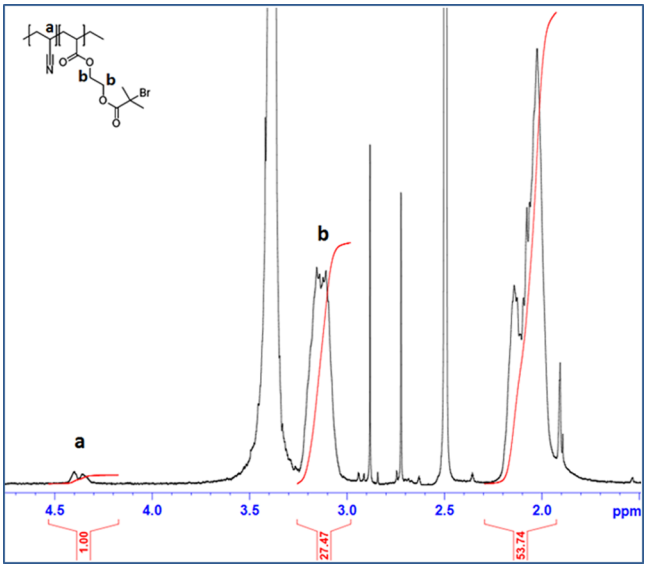

Figure 2. ^{1}H NMR spectrum of macroinitiator 144:1 P(ACN-*r*-BBEM) (compound **3** in Figure 1).

To estimate the molar masses of P(ACN-*r*-BBEM) copolymers, DLS measurements were performed on 1 mg/mL solutions of the copolymers in DMF. The 105:1 and 144:1 P(ACN-*r*-BBEM) copolymers had hydrodynamic radii of 16.6 ± 2.3 and 13.6 ± 1.1 nm, respectively. These were converted to relative molar masses calculated using the Mark−Houwink equation[60] based on polyacrylonitrile standards in DMF[61] (Supporting Information, section S1.1). These radii were found to correspond to molar masses of 4.67×10^4 and 3.33×10^4 g/mol for 105:1 and 144:1 P(ACN-*r*-BBEM) copolymers, respectively. It should be noted that these molar masses are relative values of polymer chains of equivalent hydrodynamic radius.

To obtain the final product, PAN-*g*-SPMA, photoswitchable SPMA side chains were initiated from the Br atoms along the backbone using atom transfer radical polymerization (ATRP). Two batches of this copolymer were prepared, labeled SPMA12 and SPMA20, featuring side chains with respectively 12 and 20 SPMA repeat units on average. The compositions of the products and reaction mixtures are shown in Table 2. An example ^{1}H NMR spectrum with relevant peaks marked is shown in Figure 3. All peaks with chemical shifts >5 ppm were assigned to SP units, with nine protons per SP unit appearing in that region.[59] All monomer units had a peak corresponding to the backbone CH protons around 3 ppm. The ratio of these peaks and the ACN:Br ratio from the backbone P(ACN-*r*-BBEM) composition were used to calculate the final copolymer composition, listed in Table 2 along with the composition of the reaction mixtures. In addition to ^{1}H NMR results, elemental analysis (EA) confirmed the successful incorporation of initiating Br atoms into the macroinitiator and that the ATRP polymerization of SPMA units had been successfully initiated from the macroinitiator (Supporting Information, section S2).

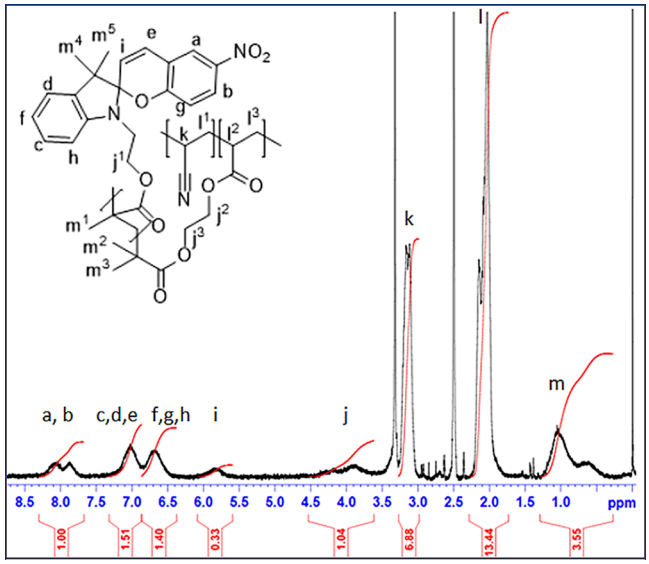

Figure 3. ^{1}H NMR spectrum of the comb copolymer SPMA12 (compound **4** in Figure 1). Peak assignments were adopted from the work of Raymo et al.[59]

The molar masses of the comb copolymers were estimated using the calculated molar masses of the backbone copolymers described above. Using the backbone:side chain weight ratios of 47:53 and 40:60 for SPMA12 and SPMA20 copolymers (Table

Table 2. Compositions of the Reaction Mixture and Product Comb Copolymers[a]

polymer name	reaction mixture composition				reaction time (h)	yield (g)	copolymer composition	
	P(ACN-*r*-BBEM) backbone	SPMA	CuCl	PMDETA			(ACN-*r*-BBEM):SPMA wt ratio	Br:SPMA mol ratio
SPMA12	0.7 g (105:1)	0.8 g	18.7 mg	58 mg	20	1.01	47:53	1:12
SPMA20	0.43 g (144:1)	0.77 g	5.3 mg	30 mg	20	1.0	40:60	1:20

[a]The macroinitiator composition (see Table 1) used in each comb copolymer is indicated in parentheses below the macroinitiator mass.

DOI: 10.1021/acsami.7b01585
ACS Appl. Mater. Interfaces 2017, 9, 13619−13631

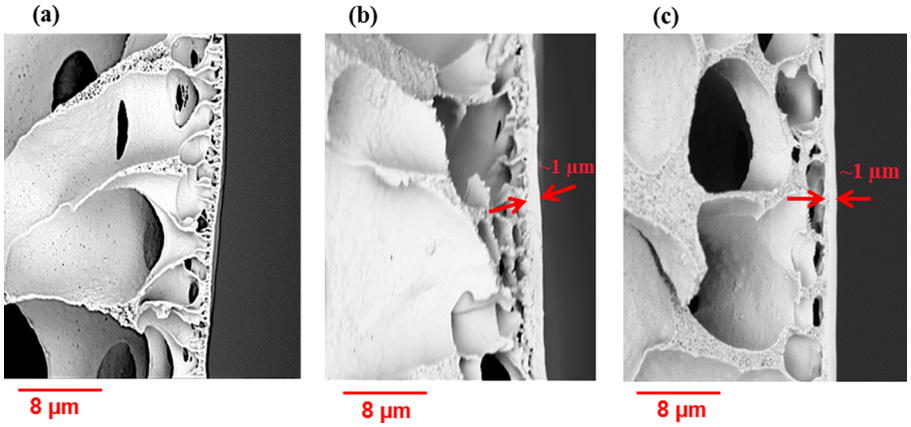

Figure 4. Cross-sectional SEM images of (a) uncoated PVDF400R base, (b) PVDF400R base coated with SPMA12 copolymer (membrane encoded M-SPMA12), and (c) PVDF400R base coated with SPMA20 copolymer (membrane encoded M-SPMA20).

2), their molar masses were estimated to be 9.91×10^4 and 8.33×10^4 g/mol, respectively (Supporting Information, section S1.2).

3.2. Preparation of Thin Film Composite (TFC) Membranes with Photoresponsive Comb Copolymer Selective Layers. We have successfully prepared TFC membranes by coating a thin layer of the comb-shaped photoresponsive copolymers on a commercial PVDF400R ultrafiltration (UF) membrane. In these TFC membranes, the comb copolymer coating serves as the selective layer that determines the effective pore size of the membrane. The base PVDF400R membrane simply serves as mechanical support. Cross-sectional SEM images of the uncoated PVDF400R base membrane and the coated membranes are shown at the same magnification (10,000×) in Figure 4. The coating layer can be observed for both membranes. It is dense (i.e., without macroscopic pores) with a thickness of approximately 1 μm. Surface SEM images were also acquired for both M-SPMA12 and M-SPMA20 membranes in each form (Supporting Information, section S3) and exhibited no large pores or defects. The coating layer adhered well to the base membrane, through partial penetration of the polymer into the membrane pores and through intermolecular interactions. No delamination was observed throughout the study.

3.3. Photoresponsive Switching of the TFC Membranes. The switching of the SPMA side chains between SP and MC forms in the comb copolymer selective layers of the membranes can be observed visually, because the SP and MC forms of these functional groups are of different colors due to differences in their conjugated structures. The zwitterionic MC form is deep purple, whereas the hydrophobic SP form appears yellow. This enables us to qualitatively observe the response of the copolymer without the need for additional instrumentation. In these experiments, the M-SPMA12 membrane was observed to respond more quickly to both visible and UV irradiation. In Figure 5, the picture on the left shows the light pink surface of the M-SPMA12 membrane prior to any phototreatment (as-coated state). This indicates that the polymer in this state contains some but not all functional groups in the MC form. Past studies show that in highly polar solvents, SPMA polymers exist with higher fractions of functional groups in MC form.[62] The solvent selected for preparing these coatings, DMSO, is a highly polar solvent, which likely led to the final color of the coating. Preliminary experiments with other coating solvents (e.g., dichloromethane) indeed showed that coatings prepared

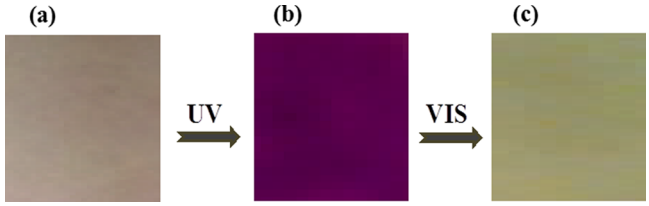

Figure 5. Photographs of the M-SPMA12 membrane surface: image taken (a) prior to any photo treatment, (b) after 1 h of UV irradiation, and (c) after 1 h of visible light irradiation.

from less polar solvents often appeared more yellowish (data not shown). Thus, the coating solvent has a visible effect on the MC/SP ratio of the functional groups in the polymer even after the solidification of the coating.

When the membrane was exposed to UV light at 254 nm wavelength for 1 h, the membrane surface turned completely purple, indicative of MC formation. This MC-dominated surface was then exposed to visible light for 1 h again, which led to the yellow membrane surface with SP configuration of polymeric chains. Similar changes were observed in the case of the M-SPMA20 membrane, although both UV and visible light exposure periods had to be extended to 2 h due to observed slower kinetics of the switch.

ATR-FTIR was used to further characterize the photo-induced conversion of SP to MC on membranes. The ATR-FTIR spectra (Figure 6) were first collected on the as-coated membranes, followed by measurements on the same sample upon UV and visible light irradiation in two consecutive cycles, each involving 1 h of exposure for M-SPMA12 and 2 h of exposure for M-SPMA20. Fingerprint IR peaks of particular importance pertinent to ring-closed SP and ring-opened MC forms are listed in Table 3.

In both membranes, the SP-specific absorbance bands of N–C_{spiro}–O at 956 cm^{-1} and C–O–C at 1090 cm^{-1} decrease in intensity during the first UV irradiation and increase back upon visible light irradiation, confirming the changes in SP population in response to light. The higher intensity of these bands in the as-coated and visible-irradiated surfaces shows that both consist mainly of SP groups. Upon UV exposure, SP groups are converted to MC form, as exhibited by a decrease in the intensity of these two peaks. Even after the first UV + visible irradiation cycle, both M-SPMA12 (Figure 6a) and M-SPMA20 (Figure 6b) can convert back to the MC form upon UV exposure. However, the structure stabilizes there, showing

DOI: 10.1021/acsami.7b01585
ACS Appl. Mater. Interfaces 2017, 9, 13619–13631

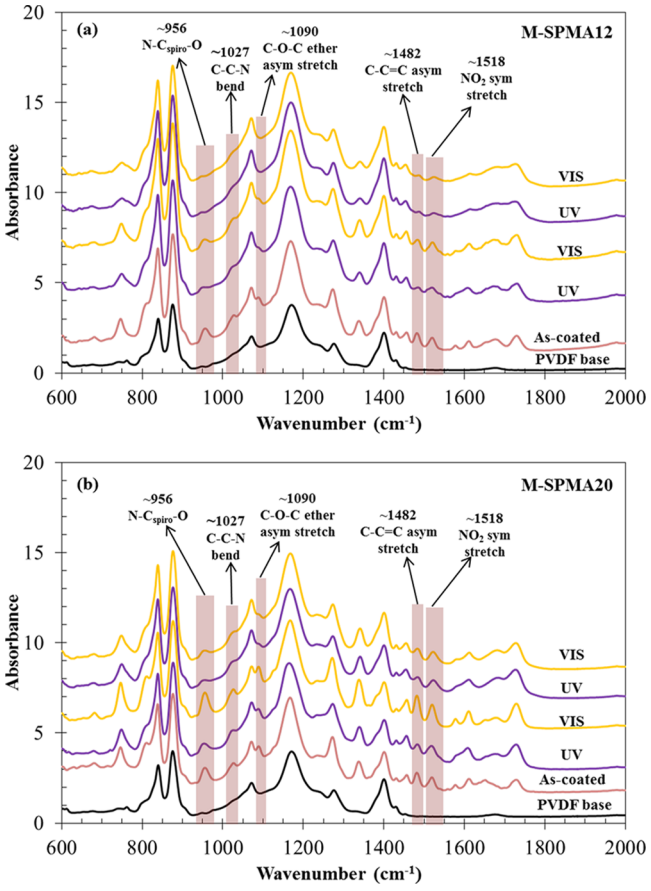

Figure 6. FTIR spectra of the as-coated and UV- and visible light-irradiated samples (a) M-SPMA12 and (b) M-SPMA20.

Table 3. Important FTIR Frequencies of PAN-*g*-SPMA Polymer in SP and MC Forms[a]

	wavenumbers (cm^{-1})	
assignment	spiropyran	merocyanine
N—C$_{spiro}$—O	956	
C—C—N bend	1027	
C—O—C ether asym stretch	1090	
C—C═C asym stretch	1482	1482
NO$_2$ sym stretch	1518	1518

[a]Peak assignments were adopted from the works of Fries et al.[63] and Dattilo et al.[64]

no further molecular rearrangement in response to light treatment.

The chemical surrounding of the SP molecules has a significant effect on the kinetics of the reversing from MC to SP, and it is known that a more hydrophilic environment stabilizes the MC form.[65,66] For a filtration membrane to be deployed in water treatment, the slow ring-closing kinetics of the zwitterionic MC form toward the SP form and the photostability of the MC form are highly favored attributes, because they would increase the operational life span of the hydrophilic membrane surface after the on-demand formation of the MC state surface. Whereas these FTIR studies indicate that the reversibility of the SP/MC switch declines in time due to fatigue, our preliminary studies on reversibility kinetics show that a higher number of switching cycles is potentially feasible. Color change on the membrane surface is observed at exposure times as short as 30 s, as opposed to the 1−2 h exposure periods used in the ATR-FTIR studies. Thus, either a stable MC state of the membrane or a higher number of switching cycles can be attained depending on the desired application by adjusting the light exposure period. For an on-demand self-cleaning system as designed in this study, a sustainable hydrophilic MC state would be desirable after the release of unwanted foulant molecules upon UV exposure, and thus the exposure periods were kept long (1 h for M-SPMA12 and 2 h for M-SPMA20) to ensure a sustainable hydrophilic surface dominated by MC molecules.

3.4. Water Permeability Change of the TFC Membranes. In addition to changes in surface hydrophilicity, the switch from the SP form to the MC form is expected to change the conformation of the side chains of the copolymer in water. The MC form will be more swollen in water, whereas the SP form would be rather collapsed. This may cause changes in membrane permeability and selectivity. In addition, water is expected to plasticize the MC form of the copolymer due to its hydrophilicity. This implies that, upon the first UV exposure, the copolymer may be able to undergo a specific rearrangement. To determine if the water permeability of the membranes changes upon the switching of the photoresponsive groups between their two forms, we measured the water flux through the TFC membranes before and after exposure to light.

First, the water permeability through the as-coated membrane was measured. Then, the same membrane swatch was subjected to two successive UV and visible light exposure cycles (1 h for M-SPMA12 and 2 h for M-SPMA20), and the water permeability was measured after each exposure. Figure 7

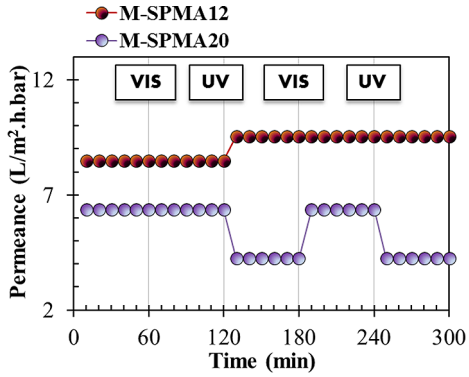

Figure 7. Water permeability changes of the M-SPMA12 and M-SPMA20 membranes.

shows that the initial visible light treatment did not lead to any change in permeability for either membrane. On the other hand, an increase in the permeability of the M-SPMA12 membrane, to 112% of its original value, was observed upon first UV irradiation. Despite the successive visible and UV exposures that followed, water permeability did not show any further change, proving membrane performance robust. M-SPMA20 showed a reversible initial decrease in its permeability upon UV irradiation, to 67% of its original value. In this case, the permeability change was found switchable for another cycle of visible and UV treatments. This conformational rearrangement of SPMA chains induced by the photochromic switch is reflected in changes to solute rejection by the membranes consistent with the changes in flux, discussed in more detail in the next section.

DOI: 10.1021/acsami.7b01585
ACS Appl. Mater. Interfaces 2017, 9, 13619−13631

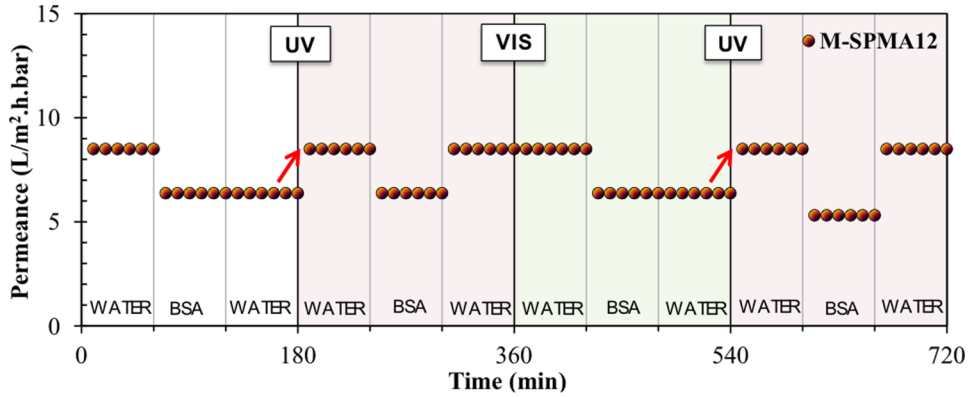

Figure 8. Fouling resistance and self-cleaning performance of the M-SPMA12 membrane.

The short side-chain length of this copolymer is likely the cause of this behavior. The 12 repeat unit side chains show a much smaller difference in end-to-end distance upon switching between collapsed and highly expanded states. This chain length is likely quite short to achieve a truly Gaussian chain, especially given the large side groups limiting chain flexibility. The end-to-end distance of a fully extended, all-trans 12-mer of SPMA can be calculated to be 3.0 nm by assuming a C−C bond length of 0.154 nm and a bond angle of 109°. The root-mean-square (RMS) end-to-end distance of a polymer in its unperturbed state, such as that in bulk, can be calculated from

$$\langle r^2 \rangle_0^{1/2} = c_\infty^{1/2} n^{1/2} l \quad (2)$$

where $\langle r^2 \rangle_0^{1/2}$ is the unperturbed RMS end-to-end distance, c_∞ is the characteristic ratio, n is the number of links (twice the degree of polymerization for a vinyl polymer), and l is the bond length.[60] Although we could not find the c_∞ value for SPMA, the values for other methacrylates with large side groups (e.g., poly(2-triphenylmethoxy)ethyl methacrylate) range between 14 and 19.[67] The unperturbed end-to-end distance for a 12-mer of SPMA can be calculated to be 3.3 nm using c_∞ = 19, which is higher than the fully extended chain end-to-end distance. Side chains of SPMA12 are therefore too short to show Gaussian behavior. It is likely that these side chains are mostly extended due to short-range interactions between the bulky SPMA side groups and are unlikely to show significant variations in end-to-end distance upon changes in solvent quality. We hypothesize that this is why no significant reversible changes were observed in the pore size of M-SPMA12 upon irradiation with UV light. Pore size changes mediated by swelling/deswelling transitions of the responsive polymer chains, which are the most common mode of responsive behavior in membranes, are unlikely to be prevalent in this system due to the short side-chain length. In contrast, we propose that longer SPMA chains are more flexible and have increased capability to change their conformation reversibly, leading to the changes in permeance and rejection documented here.

3.5. Protein Rejection, Fouling, and Self-Cleaning by Light Exposure. To demonstrate that the designed membranes can perform an on-demand removal of preformed fouling layers by simple UV exposure and that they can maintain stable pore size and permeance throughout, we conducted cyclic fouling reversibility or, in other words, self-cleaning tests. For quantifying these features, we performed dead-end stirred cell filtration tests with a protein solution frequently used for characterizing fouling potential, 1 g/L BSA in PBS.[68,69] However, prior to the self-cleaning tests, we intended to examine protein release from the membrane surface and determine any potential dissolution of the UV-induced MC state of the copolymer from the membrane surface into the PBS solution. Whereas the UV-exposed copolymer was stable in DI water, the water solubility of zwitterion-containing compounds increases with increasing ionic strength, an effect termed the anti-polyelectrolyte effect.[70−72] Thus, the copolymer may be partially soluble in high ionic strength solutions such as PBS, even if it is insoluble and stable in deionized water. To prevent protein aggregation, fouling experiments have to be conducted with BSA dissolved in PBS, so it is important to confirm the stability of the membrane selective layers in this saline solution.

We performed time-dependent UV irradiation experiments on a prefouled as-coated membrane surface covered with a thin layer of PBS solution. First, the BSA foulant solution (1 g/L BSA in PBS) was filtered for 2 h after overnight stabilization with DI water at 30 psi (0.21 MPa). After that, the membrane surface covered with a thin layer of PBS solution (3 mL) was exposed to UV light for 5 min. The solution covering the membrane was analyzed after each 5 min UV exposure period using UV−visible spectrophotometry to determine contents released from the membrane surface up to a total exposure period of 280 min.

The time-dependent absorbance spectra of the PBS solution covering the M-SPMA12 membrane (Supporting Information, Figure S2) show that solely BSA is released from the membrane surface for the complete UV exposure period of 280 min. This indicates that self-cleaning occurs, as shown by the release of the BSA from the membrane surface, but the SPMA12 polymer in its MC form does not dissolve in PBS. In addition, the stability of the MC form M-SPMA12 membrane during PBS filtration was confirmed by sequentially filtering water, PBS, and water again. No change in permeance was observed (Supporting Information, Figure S3). This indicates that both MC and SP forms of the SPMA12 copolymer are stable in PBS, and the M-SPMA12 membrane is suitable for UV-stimulated self-cleaning even in saline environments. On the other hand, the absorbance spectra of the PBS solution covering M-SPMA20 (Supporting Information, Figure S2) show peaks pertinent to the SPMA20 copolymer after a 200 min UV exposure. This indicates the solubility of MC state SPMA20 copolymer in PBS, hindering the use of M-SPMA20 as a light-responsive self-cleaning membrane in saline environments. The UV exposure time applied in this set of experiments was 2 h, determined visually from the surface color change, to maximize the MC presence on the membrane surface. In this case, the

DOI: 10.1021/acsami.7b01585
ACS Appl. Mater. Interfaces 2017, 9, 13619−13631

copolymer lost from the MC state surface of the M-SPMA20 membrane in saline environments would result in gradual thinning of the coating layer and lead to poor membrane stability and performance.

Self-cleaning studies involved several fouling−rinse−irradiation cycles, through which both the fouling potential of the MC and SP states of the copolymer were evaluated and the removal of the foulant layer was documented. The membrane was first stabilized by filtering DI water. The initial DI water permeability was recorded. PBS solution was then filtered through the membranes for 2 h, to account for any potential effects of this ionic strength change and condition the membrane. Then, 1 g/L BSA in PBS was filtered for 2 h, during which the flux was monitored. The membrane was rinsed with PBS and then PBS and DI water were filtered again. The difference between the initial and final DI water fluxes indicates irreversible/adsorptive fouling propensity. To test the actual self-cleaning capability, the fouled membranes immersed in water were exposed to UV light (1 h for M-SPMA12 and 2 h for M-SPMA20). This complete procedure was repeated four times, starting from the as-coated state and, after each fouling cycle, subjecting the surface to either UV or visible light on alternate cycles. Tests were performed on both M-SPMA12 (Figure 8) and M-SPMA20 (Supporting Information, Figure S4) membranes in addition to the base PVDF membrane used as a control (Supporting Information, Figure S5). The water flux of PVDF400R declined to 62% of its original value and did not show any increase in response to UV irradiation. In addition, BSA rejection was calculated in each fouling cycle to determine the light-triggered changes in selectivity (Table 4).

Table 4. BSA Rejection of the M-SPMA12 and M-SPMA20 Membranes

	BSA rejection (%)	
fouling cycle	M-SPMA12	M-SPMA20
1	97	93
2	92	96
3	93	95
4	93	93

Figure 8 shows that the as-coated M-SPMA12 fouled in the first fouling cycle, with its water flux decreasing to 75% of its original value. Interestingly, the membrane returned to its initial water flux upon first UV exposure, indicating removal of the foulant layer and recovery of initial membrane performance. In addition, this UV-induced MC state of the membrane surface, despite its as-coated state, showed excellent resistance to irreversible fouling by BSA, proving the MC-dominated membrane was fouling resistant for a significant time period even after the on-demand surface cleaning. A subsequent visible light exposure switched the surface back to its initial SP form, which was evidenced by fouling results similar to that of the as-coated state. When the next UV exposure followed, the result obtained was the same as that observed in the first UV exposure: complete flux recovery and a very fouling resistant surface afterward.

BSA rejection values obtained from each fouling cycle (Table 4) indicate that the pore size increases after the first UV exposure, paralleling the UV-induced water flux increase discussed in the previous section (Figure 7). After that, BSA rejection remained within a tight range through the next two fouling cycles performed.

The self-cleaning ability of the M-SPMA12 membrane upon UV exposure arises from two mechanisms: an increase in surface hydrophilicity (chemical) and a change/movement in surface morphology (mechanical). As a control experiment to demonstrate the presence of both of these mechanisms, we tested if the water flux of a fouled membrane surface in its MC form can self-clean upon exposure to visible light. In this experiment, there is no chemical self-cleaning; the surface becomes less hydrophilic upon visible light exposure, so we would expect the foulants to adsorb more strongly to the surface. However, the morphological/conformational changes to the membrane surface occur in both types of transitions (MC to SP or SP to MC). Thus, this experiment isolates the effects of the "mechanical" self-cleaning, not previously reported in other systems.

For this purpose, we first converted an M-SPMA12 membrane to its MC state by UV exposure. Then, we subjected it to a longer, 24 h, BSA fouling test and observed if any water flux recovery can be achieved by exposure to visible light. In this set of experiments, we followed the consecutive steps (1) filter DI water through the as-coated M-SPMA12 membrane for 2 h to determine the initial flux, (2) irradiate the membrane surface with UV light and then filter DI water again, (3) filter 1 g/L BSA in PBS solution for 24 h to simulate protein fouling, (4) filter DI water again to determine fouling propensity, and (5) irradiate the membrane surface with visible light and then filter DI water again. Figure 9 shows the filtration

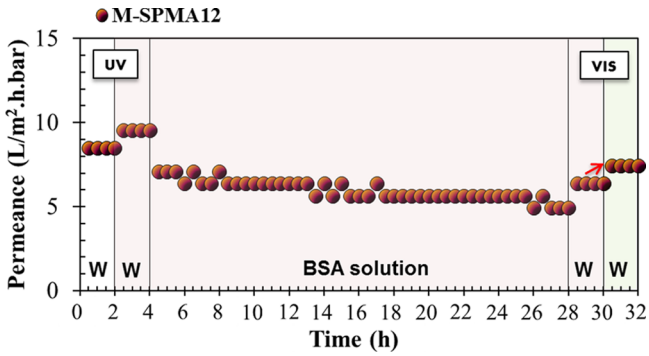

Figure 9. Visible light induced self-cleaning in the M-SPMA12 membrane. "W" stands for water.

data for only the last 2 h of recorded 24 h BSA filtration data, for the sake of clarity. Even though the 2 h BSA filtration did not result in any decline in the flux of the MC state M-SPMA12 membrane (Figure 8), the longer, 24 h, BSA filtration led to a 33% decline in the water flux that was not reversed by a water rinse (Figure 9). Afterward, the fouled membrane surface was exposed to visible light for 1 h. This exposure afforded partial flux recovery. This finding suggests a self-cleaning mechanism driven by the light-induced switch between MC and SP states, regardless of the direction in switch between MC and SP states. The self-cleaning behavior observed for this system, where the surface became less hydrophilic but also experienced a morphological change, demonstrates a novel mechanism that has a mechanical component in addition to the changes in hydrophilicity. It is also the first report, to our knowledge, of self-cleaning performance accompanied by a decrease in hydrophilicity.

The as-coated M-SPMA20 membrane showed fouling in the first cycle with its water flux decreasing to 67% of its original

DOI: 10.1021/acsami.7b01585
ACS Appl. Mater. Interfaces 2017, 9, 13619−13631

value (Supporting Information, Figure S4). However, the flux rose to a level above its initial value when the membrane was exposed to UV light after the first fouling cycle. This flux increase, stemming from the MC state SPMA20 copolymer dissolution in PBS, did not match the UV-induced flux decline observed in the previous section (Figure 7). In successive fouling cycles, visible or UV treatment appeared to offer partial recovery in flux; nevertheless, these results were deemed not reliable due to the discussed dissolution effect. On the other hand, in line with this UV-induced flux decline in the previous section, pore shrinkage upon UV exposure was manifest through the increase in BSA rejection from 93 to 96% (Table 4) between the as-coated and UV-induced MC states. Assuming a continuous, defect-free selective layer is present in all experiments, these rejection values should be independent of selective layer thickness. Thus, these results indicate that the SPMA side chains in the copolymer change their conformation as they switch between MC and SP states. The longer side-chain length in this copolymer is likely the reason such changes are observed. The side-chain length of SPMA12 is possibly too short for the changes in side-chain end-to-end distance to be significant enough in comparison with the membrane pore size to affect the rejection of BSA.

3.6. Changes in Surface Hydrophilicity and Morphology upon Light Exposure. To gain more insight into photochromic changes in surface chemistry and morphology, we performed contact angle (CA) measurements. The static CA of the PVDF400R membrane was found to be 92 ± 6°, confirming a very hydrophobic base surface. Due to its zwitterionic structure, the MC form of the spiropyran functional group is much more hydrophilic than its SP form.[64] The static CA (Figure 10) was measured first on the

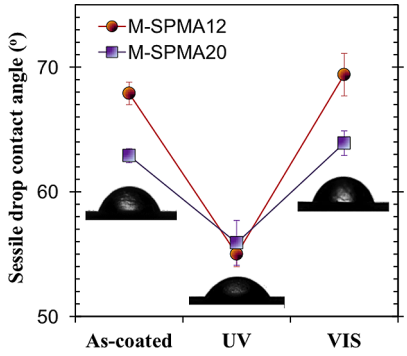

Figure 10. Static contact angle of the as-coated and UV- and visible light-irradiated membranes.

as-coated membrane, followed by measurements on the same sample upon UV and visible light irradiation, respectively. Advancing (θ_A) and receding (θ_R) angles were also measured (Table 5). The CA of both M-SPMA12 and M-SPMA20 membranes decreased in response to UV irradiation, indicating a sharp increase in hydrophilic wettability. For M-SPMA12, the static CA was 68 ± 1° (θ_A = 81 ± 1° and θ_R = 42 ± 2°) on the as-coated surface and decreased to 55 ± 1° (θ_A = 70 ± 1° and θ_R = 21 ± 2°) after UV irraditation. For M-SPMA20, the static CA was 63 ± 1° (θ_A = 78 ± 3° and θ_R = 41 ± 1°) on the as-coated surface and decreased to 56 ± 2° (θ_A = 66 ± 1° and θ_R = 22 ± 2°) after UV irraditation. The wettability changes switched back after visible light irradiation, indicating that the

Table 5. Advancing and Receding Contact Angles of the As-Coated and UV- and Visible Light-Irradiated Membranes

		contact angle (deg)	
		advancing	receding
M-SPMA12	as-coated	81 ± 1	42 ± 2
	UV	70 ± 1	21 ± 2
	vis	84 ± 2	47 ± 1
M-SPMA20	as-coated	78 ± 3	41 ± 1
	UV	66 ± 1	22 ± 2
	vis	78 ± 2	45 ± 1
PVDF400R		108 ± 5	65 ± 2

hydrophilic MC form had transformed back to the hydrophobic SP form.

Most studies of photoresponsive membranes focus on changes in surface energy as the key factor in changing the fouling potential. Whereas a surface becoming more hydrophilic may lead to the removal of foulants, this effect may be limited by physical/mechanical factors. Proteins that deposit on surfaces often denature and aggregate. Changes in hydrophilicity may not be sufficient to mechanically remove these deposited layers. Photoresponsive polymers, however, may also undergo physical and morphological changes upon exposure to light. In addition to the changes in surface chemistry, we expect the switch between SP and MC forms of the side-chain pendant groups to affect the conformation and behavior of the copolymer side chains. This movement on the membrane surface, enabled by the comb architecture that does not constrain the photochromic side chains, is expected to contribute to the self-cleaning performance. To our knowledge, this contribution to photoinduced self-cleaning has not yet been studied in photoresponsive membranes.

To document that the light exposure causes the movement of polymer chains on the membrane surface, we performed AFM on the self-cleaning M-SPMA12 membrane in the as-coated and UV- and visible light-irradiated states and monitored the changes in the surface morphology and roughness. Figure 11 shows that the surface morphology of the UV-treated membrane is drastically different from both the as-coated and visible light-treated membranes. The UV-treated surface features closely packed fine heights with pointed ends atop, where the visible light-treated surface shows rather a variant hill-and-valley type topography with a broad and rounded contour. On the other hand, the as-coated surface displays a patchwork of both structures, implying the compositional copresence of SP and MC forms on the surface. RMS roughness results (Figure 12) follow a similar trend; the as-coated and visible light-treated membranes show RMS roughness values of 28 ± 2 and 27 ± 2 nm, respectively. The similarity between these morphologies is consistent with other data that show that the as-coated surface predominantly comprises the SP form. As expected, the UV-treated surface shows a very different roughness, 45 ± 4 nm, significantly higher than those of the others. These changes suggest that when the copolymer side chains switch from the SP to the MC state, the conformational changes induce a reorganization in morphology and a motion on the membrane surface. This motion may promote the removal of a foulant layer by deforming it and breaking it apart.

DOI: 10.1021/acsami.7b01585
ACS Appl. Mater. Interfaces 2017, 9, 13619−13631

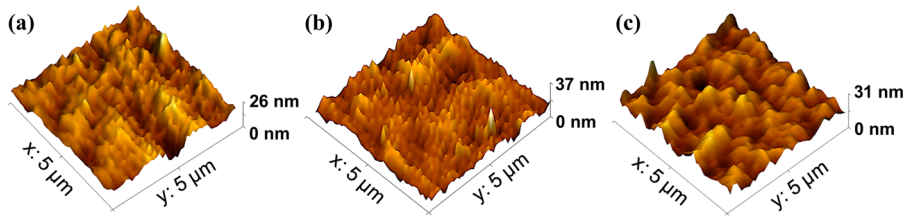

Figure 11. AFM images of the M-SPMA12 at (a) as-coated, (b) UV-irradiated, and (c) visible light-irradiated states.

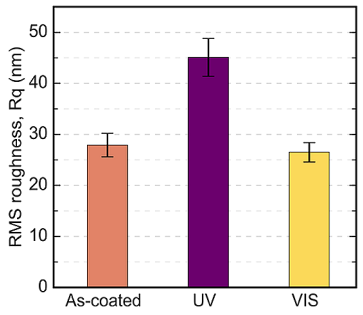

Figure 12. RMS surface roughness values of the M-SPMA12 membrane at as-coated, UV-irradiated, and visible light-irradiated states.

Surface roughening improves the wetting properties of a solid material with a positive wetting tendency,[73] which applies to the membranes of this study. This implies that the increase in surface roughness observed in the M-SPMA12 membrane when switched from SP to MC form likely contributes to the decrease in contact angle in addition to the more hydrophilic surface chemistry.

4. CONCLUSION

In this paper, we demonstrated a new self-cleaning, photoresponsive membrane that can remove predeposited foulant layers upon exposure to UV light. The membrane exhibits UV-triggered surface morphology changes, and it sustains stable pore size and permeance after UV treatment. We synthesized novel comb-shaped graft copolymers with polyacrylonitrile (PAN) backbones and photoreactive spiropyran methacrylate (SPMA) side chains using atom transfer radical polymerization (ATRP) at two side-chain lengths. The side chains undergo a light-induced transition between a hydrophobic spiropyran (SP) state and a zwitterionic, hydrophilic merocyanine (MC) state, allowing photoregulated control over membrane features. We used these comb-shaped copolymers to produce thin film composite (TFC) membranes by coating a commercial PVDF membrane with a thin layer of the copolymer solution. Changes in fingerprint IR peaks indicative of SP and MC forms upon light treatment were used to confirm the structural difference between the two forms at a molecular level. The as-coated membrane surface was found to consist mainly of the hydrophobic SP groups prior to any phototreatment. These hydrophobic groups allowed the adsorption of hydrophobic solutes on channel walls, decreasing flow rate. When the the photochemical response was reversed by irradiation with UV light, the hydrophobic SP groups converted to the hydrophilic, zwitterionic MC groups that released the adsorbed molecules and permitted water permeation once again. We found that flux decline through a bovine serum albumin (BSA)-fouled membrane can be fully reversed back to its original value by a simple, nonmechanical intervention of exposure to UV light. The switch between MC and SP states causes morphological changes on the membrane surface as documented by atomic force microscopy (AFM). Thus, self-cleaning is attained both by increased hydrophilicity and by the motion of the membrane surface during this rearrangement, providing a mechanical push that enhances the removal of deposited foulants. The morphological changes enable self-cleaning behavior to be achieved during the switch from the MC form to the less hydrophilic SP form also, exhibited as flux recovery upon visible light exposure. Removal of foulant layers accompanied by a decrease in hydrophilicity confirms a physical/mechanical mechanism to self-cleaning. Whereas these photoresponsive copolymers were used directly as the membrane selective layer in this study, they are also promising as self-cleaning coatings for reverse osmosis and nanofiltration membranes as well as other surfaces prone to organic and biofouling such as pipes and biomaterials.

■ ASSOCIATED CONTENT

Supporting Information

The Supporting Information is available free of charge on the ACS Publications website at DOI: 10.1021/acsami.7b01585.

Section S1: Experimental details for dynamic light scattering experiments and molar mass calculations. Section S2: Elemental analysis results. Section S3: Surface morphology of the membranes by scanning electron microscopy. Section S4: Protein release in phosphate buffered saline solution and membrane stability. Section S5: Self-cleaning tests on M-SPMA20 and base PVDF400R membrane (PDF)

■ AUTHOR INFORMATION

Corresponding Author

*(A.A.) Phone: (617) 627-4681. Fax: (617) 627-3991. E-mail: Ayse.Asatekin@tufts.edu.

ORCID

Xiaoran Hu: 0000-0001-7598-4516
Samuel W. Thomas III: 0000-0002-0811-9781
Ayse Asatekin: 0000-0002-4704-1542

Notes

The authors declare no competing financial interest.

■ ACKNOWLEDGMENTS

We thank David Wilbur for help with NMR analysis, NSL Analytical Services, Inc., for performing elemental analysis, and Giovanni Perotto for help with AFM measurements and useful discussions. This research was funded by Tufts University's Tufts Collaborates Seed Grant Program and the National Science Foundation (NSF) under Grant CBET-1437772.

DOI: 10.1021/acsami.7b01585
ACS Appl. Mater. Interfaces 2017, 9, 13619−13631

REFERENCES

(1) WHO. *World Health Statistics 2010*; World Health Organization: France, 2010.

(2) Kaner, P.; Johnson, D. J.; Seker, E.; Hilal, N.; Altinkaya, S. A. Layer-by-Layer Surface Modification of Polyethersulfone Membranes Using Polyelectrolytes and AgCl/TiO_2 Xerogels. *J. Membr. Sci.* **2015**, *493*, 807−819.

(3) Lee, A.; Elam, J. W.; Darling, S. B. Membrane Materials for Water Purification: Design, Development, and Application. *Environ. Sci.: Water Res. Technol.* **2016**, *2* (1), 17−42.

(4) Werber, J. R.; Osuji, C. O.; Elimelech, M. Materials for Next-Generation Desalination and Water Purification Membranes. *Nat. Rev. Mater.* **2016**, *1*, 16018.

(5) Nunes, S. P. Block Copolymer Membranes for Aqueous Solution Applications. *Macromolecules* **2016**, *49* (8), 2905−2916.

(6) Pabby, A. K.; Rizvi, S. S. H.; Sastre, A. M. Membrane Applications in Biotechnology, Food Processing, Life Sciences, and Energy Conversion: Introduction. In *Handbook of Membrane Separations: Chemical, Pharmaceutical, Food, and Biotechnological Applications*; Pabby, A. K., Sastre, A. M., Rizvi, S. S. H., Eds.; CRC Press: Boca Raton, FL, USA, 2015; pp 483−484.

(7) Mohammad, A. W.; Ng, C. Y.; Lim, Y. P.; Ng, G. H. Ultrafiltration in Food Processing Industry: Review on Application, Membrane Fouling, and Fouling Control. *Food Bioprocess Technol.* **2012**, *5* (4), 1143−1156.

(8) Kaner, P.; Bengani-Lutz, P.; Sadeghi, I.; Asatekin, A. Responsive Filtration Membranes by Polymer Self-Assembly. *Technology* **2016**, *4* (4), 1−12.

(9) Baker, R. W. *Membrane Technology and Applications*, 2nd ed.; Wiley: New York, 2004; pp 257−273.

(10) Asatekin, A.; Vannucci, C. Self-Assembled Polymer Nanostructures for Liquid Filtration Membranes: A Review. *Nanosci. Nanotechnol. Lett.* **2015**, *7* (1), 21−32.

(11) Hong, S.; Elimelech, M. Chemical and Physical Aspects of Natural Organic Matter (NOM) Fouling of Nanofiltration Membranes. *J. Membr. Sci.* **1997**, *132*, 159−181.

(12) Goosen, M. F. A.; Sablani, S. S.; Al-Hinai, H.; Al-Obeidani, S.; Al-Belushi, R.; Jackson, D. Fouling of Reverse Osmosis and Ultrafiltration Membranes: A Critical Review. *Sep. Sci. Technol.* **2004**, *39* (10), 2261−2297.

(13) Nystroem, M.; Kaipia, L.; Luque, S. Fouling and Retention of Nanofiltration Membranes. *J. Membr. Sci.* **1995**, *98*, 249−262.

(14) Wandera, D.; Wickramasinghe, S. R.; Husson, S. M. Stimuli-Responsive Membranes. *J. Membr. Sci.* **2010**, *357* (1), 6−35.

(15) Gan, L.; Gan, Y.; Deen, G. R. Poly(N-acryloyl-N′-propylpiperazine): A New Stimuli-Responsive Polymer. *Macromolecules* **2000**, *33* (21), 7893−7897.

(16) Nakayama, M.; Okano, T. Intelligent Thermoresponsive Polymeric Micelles for Targeted Drug Delivery. *J. Drug Delivery Sci. Technol.* **2006**, *16* (1), 35−44.

(17) Yang, B.; Yang, W. Novel Pore-Covering Membrane as a Full Open/Close Valve. *J. Membr. Sci.* **2005**, *258* (1), 133−139.

(18) Himstedt, H. H.; Marshall, K. M.; Wickramasinghe, S. R. pH-Responsive Nanofiltration Membranes by Surface Modification. *J. Membr. Sci.* **2011**, *366* (1), 373−381.

(19) Yang, Q.; Himstedt, H. H.; Ulbricht, M.; Qian, X.; Wickramasinghe, S. R. Designing Magnetic Field Responsive Nanofiltration Membranes. *J. Membr. Sci.* **2013**, *430*, 70−78.

(20) Murdan, S. Electro-Responsive Drug Delivery from Hydrogels. *J. Controlled Release* **2003**, *92* (1−2), 1−17.

(21) Lee, K.; Asher, S. A. Photonic Crystal Chemical Sensors: pH and Ionic Strength. *J. Am. Chem. Soc.* **2000**, *122* (39), 9534−9537.

(22) Yoshida, R.; Uesusuki, Y. Biomimetic Gel Exhibiting Self-Beating Motion in ATP Solution. *Biomacromolecules* **2005**, *6* (6), 2923−2926.

(23) Juodkazis, S.; Mukai, N.; Wakaki, R.; Yamaguchi, A.; Matsuo, S.; Misawa, H. Reversible Phase Transitions in Polymer Gels Induced by Radiation Forces. *Nature* **2000**, *408* (6809), 178−181.

(24) Plamper, F. A.; Walther, A.; Müller, A. H.; Ballauff, M. Nanoblossoms: Light-Induced Conformational Changes of Cationic Polyelectrolyte Stars in the Presence of Multivalent Counterions. *Nano Lett.* **2007**, *7* (1), 167−171.

(25) Hu, X.; McIntosh, E.; Simon, M. G.; Staii, C.; Thomas, S. W., III. Stimuli-Responsive Free-Standing Layer-By-Layer Films. *Adv. Mater.* **2016**, *28*, 715−721.

(26) Liu, Z.; Wang, W.; Xie, R.; Ju, X.-J.; Chu, L.-Y. Stimuli-Responsive Smart Gating Membranes. *Chem. Soc. Rev.* **2016**, *45*, 460−475.

(27) Sinha, M.; Purkait, M. Preparation and Characterization of Novel Pegylated Hydrophilic pH Responsive Polysulfone Ultrafiltration Membrane. *J. Membr. Sci.* **2014**, *464*, 20−32.

(28) Sinha, M.; Purkait, M. Preparation of a Novel Thermo Responsive PSF Membrane, with Cross Linked PVCL-co-PSF Copolymer for Protein Separation and Easy Cleaning. *RSC Adv.* **2015**, *5* (29), 22609−22619.

(29) Sommer, S.; Ekin, A.; Webster, D. C.; Stafslien, S. J.; Daniels, J.; VanderWal, L. J.; Thompson, S. E.; Callow, M. E.; Callow, J. A. A y Preliminary Study on the Properties and Fouling-Release Performance of Siloxane−Polyurethane Coatings Prepared from Poly-(dimethylsiloxane) (PDMS) Macromers. *Biofouling* **2010**, *26* (8), 961−972.

(30) Krishnan, S.; Wang, N.; Ober, C. K.; Finlay, J. A.; Callow, M. E.; Callow, J. A.; Hexemer, A.; Sohn, K. E.; Kramer, E. J.; Fischer, D. A. Comparison of the Fouling Release Properties of Hydrophobic Fluorinated and Hydrophilic PEGylated Block Copolymer Surfaces: Attachment Strength of the Diatom Navicula and the Green Alga Ulva. *Biomacromolecules* **2006**, *7* (5), 1449−1462.

(31) Yarbrough, J. C.; Rolland, J. P.; DeSimone, J. M.; Callow, M. E.; Finlay, J. A.; Callow, J. A. Contact Angle Analysis, Surface Dynamics, And Biofouling Characteristics of Cross-Linkable, Random Perfluoropolyether-Based Graft Terpolymers. *Macromolecules* **2006**, *39* (7), 2521−2528.

(32) Colak, S.; Tew, G. N. Amphiphilic Polybetaines: The Effect of Side-Chain Hydrophobicity on Protein Adsorption. *Biomacromolecules* **2012**, *13* (5), 1233−1239.

(33) Holmlin, R. E.; Chen, X. X.; Chapman, R. G.; Takayama, S.; Whitesides, G. M. Zwitterionic SAMs That Resist Nonspecific Adsorption of Protein from Aqueous Buffer. *Langmuir* **2001**, *17* (9), 2841−2850.

(34) Kitano, H.; Kawasaki, A.; Kawasaki, H.; Morokoshi, S. Resistance of Zwitterionic Telomers Accumulated on Metal Surfaces against Nonspecific Adsorption of Proteins. *J. Colloid Interface Sci.* **2005**, *282* (2), 340−348.

(35) Ostuni, E.; Chapman, R. G.; Liang, M. N.; Meluleni, G.; Pier, G.; Ingber, D. E.; Whitesides, G. M. Self-Assembled Monolayers That Resist the Adsorption of Proteins and the Adhesion of Bacterial and Mammalian Cells. *Langmuir* **2001**, *17* (20), 6336−6343.

(36) Park, Y. S.; Ito, Y.; Imanishi, Y. Photocontrolled gating by polymer brushes grafted on porous glass filter. *Macromolecules* **1998**, *31* (8), 2606−2610.

(37) Chung, D. J.; Ito, Y.; Imanishi, Y. Preparation of Porous Membranes Grafted with Poly(Spiropyran-Containing Methacrylate) and Photocontrol of Permeability. *J. Appl. Polym. Sci.* **1994**, *51* (12), 2027−2033.

(38) Rosario, R.; Gust, D.; Garcia, A. A.; Hayes, M.; Taraci, J. L.; Clement, T.; Dailey, J. W.; Picraux, S. T. Lotus Effect Amplifies Light-Induced Contact Angle Switching. *J. Phys. Chem. B* **2004**, *108* (34), 12640−12642.

(39) Ando, E.; Miyazaki, J.; Morimoto, K.; Nakahara, H.; Fukuda, K. J-Aggregation of Photochromic Spiropyran in Langmuir-Blodgett-Films. *Thin Solid Films* **1985**, *133* (1−4), 21−28.

(40) Nayak, A.; Liu, H. W.; Belfort, G. An Optically Reversible Switching Membrane Surface. *Angew. Chem., Int. Ed.* **2006**, *45* (25), 4094−4098.

(41) Nicoletta, F. P.; Cupelli, D.; Formoso, P.; De Filpo, G.; Colella, V.; Gugliuzza, A. Light Responsive Polymer Membranes: A Review. *Membranes* **2012**, *2* (1), 134−197.

DOI: 10.1021/acsami.7b01585
ACS Appl. Mater. Interfaces 2017, 9, 13619−13631

(42) Warshawsky, A.; Kahana, N.; Buchholtz, F.; Zelichonok, A.; Ratner, J.; Krongauz, V. Photochromic Polysulfones. 1. Synthesis of Polymeric Polysulfone Carrying Pendant Spiropyran and Spirooxazine Groups. *Ind. Eng. Chem. Res.* **1995**, *34* (8), 2825−2832.
(43) Ratner, J.; Kahana, N.; Warshawsky, A.; Krongauz, V. Photochromic Polysulfones. 2. Photochromic Properties of Polymeric Polysulfone Carrying Pendant Spiropyran and Spirooxazine Groups. *Ind. Eng. Chem. Res.* **1996**, *35* (4), 1307−1315.
(44) Kimura, K.; Sakamoto, H.; Nakamura, T. Application of Photoresponsive Polymers Carrying Crown Ether and Spirobenzopyran Side Chains to Photochemical Valve. *J. Nanosci. Nanotechnol.* **2006**, *6* (6), 1741−1749.
(45) Klajn, R. Spiropyran-Based Dynamic Materials. *Chem. Soc. Rev.* **2014**, *43* (1), 148−184.
(46) Chen, S.; Jiang, F.; Cao, Z.; Wang, G.; Dang, Z.-M. Photo, pH, and Thermo Triple-Responsive Spiropyran-Based Copolymer Nanoparticles for Controlled Release. *Chem. Commun.* **2015**, *51* (63), 12633−12636.
(47) Jiang, F.; Chen, S.; Cao, Z.; Wang, G. A Photo, Temperature, and pH Responsive Spiropyran-Functionalized Polymer: Synthesis, Self-Assembly and Controlled Release. *Polymer* **2016**, *83*, 85−91.
(48) Aznar, E.; Oroval, M.; Pascual, L.; Murguía, J. R.; Martínez-Máñez, R.; Sancenón, F. Gated Materials for On-Command Release of Guest Molecules. *Chem. Rev.* **2016**, *116* (2), 561−718.
(49) Chen, L.; Wang, W.; Su, B.; Wen, Y.; Li, C.; Zhou, Y.; Li, M.; Shi, X.; Du, H.; Song, Y. A Light-Responsive Release Platform by Controlling the Wetting Behavior of Hydrophobic Surface. *ACS Nano* **2014**, *8* (1), 744−751.
(50) Tan, B. Y. L.; Tai, M. H.; Juay, J.; Liu, Z.; Sun, D. A Study on the Performance of Self-Cleaning Oil−Water Separation Membrane Formed by Various TiO_2 Nanostructures. *Sep. Purif. Technol.* **2015**, *156*, 942−951.
(51) Xu, Q. F.; Liu, Y.; Lin, F.-J.; Mondal, B.; Lyons, A. M. Superhydrophobic TiO_2−Polymer Nanocomposite Surface with UV-Induced Reversible Wettability and Self-Cleaning Properties. *ACS Appl. Mater. Interfaces* **2013**, *5* (18), 8915−8924.
(52) Zhang, L.; Zhong, Y.; Cha, D.; Wang, P. A Self-Cleaning Underwater Superoleophobic Mesh for Oil-Water Separation. *Sci. Rep.* **2013**, *3*, 1−5.
(53) Irvine, D. J.; Ruzette, A. V. G.; Mayes, A. M.; Griffith, L. G. Nanoscale Clustering of RGD Peptides at Surfaces Using Comb Polymers. 2. Surface Segregation of Comb Polymers in Polylactide. *Biomacromolecules* **2001**, *2* (2), 545−556.
(54) Asatekin, A.; Mennitti, A.; Kang, S.; Elimelech, M.; Morgenroth, E.; Mayes, A. M. Antifouling Nanofiltration Membranes for Membrane Bioreactors from Self-Assembling Graft Copolymers. *J. Membr. Sci.* **2006**, *285*, 81−89.
(55) Kang, S.; Asatekin, A.; Mayes, A. M.; Elimelech, M. Protein Antifouling Mechanisms of PAN UF Membranes Incorporating PAN-*g*-PEO Additive. *J. Membr. Sci.* **2007**, *296* (1−2), 42−50.
(56) Asatekin, A.; Kang, S.; Elimelech, M.; Mayes, A. M. Anti-fouling Ultrafiltration Membranes Containing Polyacrylonitrile-Graft-Poly(ethylene oxide) as an Additive. *J. Membr. Sci.* **2007**, *298* (1−2), 136−146.
(57) Friedle, S.; Thomas, S. W., III. Controlling Contact Electrification with Photochromic Polymers. *Angew. Chem., Int. Ed.* **2010**, *49* (43), 7968−7971.
(58) Jones, M. W.; Gibson, M. I.; Mantovani, G.; Haddleton, D. M. Tunable Thermo-Responsive Polymer−Protein Conjugates via a Combination of Nucleophilic Thiol−Ene "Click" and SET-LRP. *Polym. Chem.* **2011**, *2* (3), 572−574.
(59) Raymo, F. M.; Giordani, S.; White, A. J.; Williams, D. J. Digital Processing with a Three-State Molecular Switch. *J. Org. Chem.* **2003**, *68* (11), 4158−4169.
(60) Young, R. J.; Lovell, P. A. *Introduction to Polymers*, 3rd ed.; CRC Press: Boca Raton, FL, USA, 1991; pp 263−264.
(61) Mori, S.; Barth, H. G. *Size Exclusion Chromatography*; Springer: Heidelberg, Germany, 2013; pp 77−114.
(62) Florea, L.; McKeon, A.; Diamond, D.; Benito-Lopez, F. Spiropyran Polymeric Microcapillary Coatings for Photodetection of Solvent Polarity. *Langmuir* **2013**, *29* (8), 2790−2797.
(63) Fries, K. H.; Driskell, J. D.; Samanta, S.; Locklin, J. Spectroscopic Analysis of Metal Ion Binding in Spiropyran Containing Copolymer Thin Films. *Anal. Chem.* **2010**, *82* (8), 3306−3314.
(64) Dattilo, D.; Armelao, L.; Fois, G.; Mistura, G.; Maggini, M. Wetting Properties of Flat and Porous Silicon Surfaces Coated with a Spiropyran. *Langmuir* **2007**, *23* (26), 12945−12950.
(65) Ercole, F.; Davis, T. P.; Evans, R. A. Photo-Responsive Systems and Biomaterials: Photochromic Polymers, Light-Triggered Self-Assembly, Surface Modification, Fluorescence Modulation and Beyond. *Polym. Chem.* **2010**, *1* (1), 37−54.
(66) Evans, R. A.; Hanley, T. L.; Skidmore, M. A.; Davis, T. P.; Such, G. K.; Yee, L. H.; Ball, G. E.; Lewis, D. A. The Generic Enhancement of Photochromic Dye Switching Speeds in a Rigid Polymer Matrix. *Nat. Mater.* **2005**, *4* (3), 249−253.
(67) Fargere, T. Synthesis of Graft Polymers from an Ozonized Ethylene-Vinyl Acetate Copolymer (EVA).1. Study of the Radical Polymerization of Styrene Initiated by an Ozonized EVA. *J. Polym. Sci., Part A: Polym. Chem.* **1994**, *32* (7), 1377−1384.
(68) Nabe, A.; Staude, E.; Belfort, G. Surface Modification of Polysulfone Ultrafiltration Membranes and Fouling by BSA Solutions. *J. Membr. Sci.* **1997**, *133* (1), 57−72.
(69) Bengani, P.; Kou, Y.; Asatekin, A. Zwitterionic Copolymer Self-Assembly for Fouling Resistant, High Flux Membranes with Size-Based Small Molecule Selectivity. *J. Membr. Sci.* **2015**, *493*, 755−765.
(70) Yang, Q.; Ulbricht, M. Novel Membrane Adsorbers with Grafted Zwitterionic Polymers Synthesized by Surface-Initiated ATRP and Their Salt-Modulated Permeability and Protein Binding Properties. *Chem. Mater.* **2012**, *24* (15), 2943−2951.
(71) Georgiev, G. S.; Karnenska, E. B.; Vassileva, E. D.; Kamenova, I. P.; Georgieva, V. T.; Iliev, S. B.; Ivanov, I. A. Self-assembly, anti polyelectrolyte effect, and nonbiofouling properties of polyzwitterions. *Biomacromolecules* **2006**, *7* (4), 1329−1334.
(72) Lowe, A. B.; McCormick, C. L. Synthesis and Solution Properties of Zwitterionic Polymers. *Chem. Rev.* **2002**, *102* (11), 4177−4190.
(73) Blossey, R. Self-Cleaning Surfaces—Virtual Realities. *Nat. Mater.* **2003**, *2* (5), 301−306.

DOI: 10.1021/acsami.7b01585
ACS Appl. Mater. Interfaces 2017, 9, 13619−13631